Received July 6, 2019, accepted July 22, 2019, date of publication July 29, 2019, date of current version August 13, 2019.

Digital Object Identifier 10.1109/ACCESS.2019.2931572

A Refined Bilateral Filtering Algorithm Based on Adaptively-Trimmed-Statistics for Speckle Reduction in SAR Imagery

JIAQIU AI[1,2,3], (Member, IEEE), RUIMING LIU[1,2], BO TANG[4], LU JIA[1,2,3], JINLING ZHAO[5], AND FANG ZHOU[1,2], (Member, IEEE)

[1]Key Laboratory of Knowledge Engineering with Big Data, Ministry of Education, Hefei University of Technology, Hefei 230009, China
[2]School of Computer Science and Information Engineering, Hefei University of Technology, Hefei 230009, China
[3]Anhui Province Key Laboratory of Industry Safety and Emergency Technology, Hefei 230009, China
[4]Department of Electrical and Computer Engineering, Mississippi State University, Mississippi, MS 39762, USA
[5]National Engineering Research Center for Agro-Ecological Big Data Analysis and Application, Anhui University, Hefei 230601, China

Corresponding author: Jiaqiu Ai (aijiaqiu1985@hfut.edu.cn)

This work was supported in part by the National Natural Science Foundation of China under Grant 61701157 and Grant 61701154, in part by the Natural Science Foundation of Anhui Province under Grant 1808085QF206, in part by the Fundamental Research Funds for the Central Universities of China under Grant PA2019GDPK0073, in part by the Open Research Fund of the National Engineering Research Center for Agro-Ecological Big Data Analysis and Application, Anhui University, and in part by the Open Research Fund of the Key Laboratory of Radar Imaging and Microwave Photonics, Nanjing University of Aeronautics and Astronautics.

ABSTRACT This paper proposes a refined bilateral filtering algorithm based on adaptively trimmed-statistics (ATS-RBF) for speckle reduction in SAR imagery. The new de-speckling method is based on the bilateral filtering method, where the similarities of gray levels and the spatial location of the neighboring pixels are exploited. However, the traditional bilateral filter is not effective to reduce the strong speckle, which is often presented as impulse noise. The ATS-RBF designs an adaptive sample trimming method to properly select the samples in the local reference window and the trimming depth used for sample trimming is automatically derived according to the homogeneity of the local reference window. Furthermore, an alterable window size-based scheme is proposed to enhance the speckle noise smoothing strength in homogeneous backgrounds. Finally, bilateral filtering is applied using the adaptively trimmed samples. The ATS-RBF has an excellent speckle noise smoothing performance while preserving the edges and the texture information of the SAR images. The experiments validate the effectiveness of the proposed method using TerraSAR-X images.

INDEX TERMS Synthetic aperture radar (SAR), speckle noise reduction, refined bilateral filtering, adaptive-trimmed-statistics, alterable window size.

LIST OF SYMBOLS AND ABBREVIATIONS

ψ	Trimmed pixels for bilateral filtering
σ_d	Geometric diffusion factor
σ_r	Photometric similarity diffusion factor
α	Trimming depth
μ_w	The mean of all the samples of local reference window
α_w	Standard deviation of all the samples of local reference window
N	The size of local reference window
σ_h	Standard deviations of the whole image
σ_h	Standard deviations of the whole image
β	Trimming strength weight
T	Expansion threshold
r_w	Window size of ATS-RBF
μ_x	Mean value of the original image
μ_y	Mean value of the filtered result
σ_x	Standard deviations of the original image
σ_y	Standard deviations of the filtered result
c_1	Coefficient used to stabilize the division
c_2	Coefficient used to stabilize the division
SRAD	Speckle reducing anisotropic diffusion
OSRAD	Oriented speckle reducing anisotropicdiffusion

The associate editor coordinating the review of this manuscript and approving it for publication was Rui Xiong.

DPAD	Detail preserving anisotropic diffusion
PRSS-SRAD	Pixel relativity speckle statistic based speckle reducing anisotropic diffusion
EPPR-SRAD	Edge probability and pixel relativity-based speckle reducing anisotropic diffusion
BM3D	Block-matching and 3-D filter
AWGN	Additive white Gaussian noise
ATS-RBF	Refined bilateral filter based on adaptive-trimmed-statistics
PUF	Pixel-under-filtering
ENL	Equivalent number of looks
ESI	Edge sustaining index
PSNR	Peak signal-to-noise ratio
MSE	Mean square error
SSIM	Structural similarity metric

I. INTRODUCTION

Synthetic aperture radar (SAR) is an active radar which has the advantages of all-time and all-weather sensing capability. With the rapid development of space-borne SAR technology, advanced SAR sensors can provide fine resolution images, such as TerraSAR-X (Germany) [1], Radarsat-2 (Canada) [2], Sentinel-1 and Envisat-ASAR (European Space Agency, ESA) [3], [4], Cosmo-SkyMed (Italy) [5], ALOS-2 (Japan) [6], TecSAR (Israel) [7], Gaofen-3 (China) [8]. SAR images are widely used both in civilian and military fields, such as marine surveillance [1], agriculture & forestry monitoring [4], disaster monitoring [3], [5], environment monitoring [8], battlefield intelligence reconnaissance [6], etc. SAR imaging is based on coherent processing of the scattered signals of the resolution cell. Consequently, it's inevitable that speckle noise appears. Speckle noise is randomly-distributed and it makes SAR images hard for interpretation and eventually influences their further applications [9].

In the past decades, with a long-term study, many speckle reduction methods are developed. There are two categories of SAR speckle reduction mechanisms, one category is the multi-look processing technique [10]–[12], the other one is the filtering technique [13]–[36].

Multi-look processing methods [10]–[12] amount to incoherently averaging a certain number of independent SAR images. They reduce the speckle noise intensity, however, such methods sacrifice a loss of the spatial resolution. As the number of looks increases, the resolution of the processed SAR images degrades. Therefore, it is preferable to develop suitable speckle noise filtering techniques. These methods reduce the speckle noise significantly and sustain all the relevant features, such as radiometric and textural information.

In the last three decades, many filtering methods, such as the mean and median filtering, have been used for SAR speckle noise filtering. However, due to the multiplicative characteristics of the SAR speckle noise, the filtering performance of the traditional mean and median filters are not promising. To solve the above problems, many adaptive local filters based on the multiplicative model have been developed. Most of the existing filters are local-statistics based spatially adaptive filters. The most representative filters are the Lee filter [13], the refined Lee filter [14], the Frost filter [15], the Kuan filter [16], and the Gamma-MAP filter [17], etc. These filters are simple and efficient, but they ruin the details such as the edge and the texture information. The idea of local statistics based filtering has been incorporated in anisotropic diffusion framework (SRAD) [18], and the improved versions of SRAD filter such as oriented speckle reducing anisotropic diffusion (OSRAD) [19], detail preserving anisotropic diffusion (DPAD) [20] were proposed later after SRAD. The pixel relativity speckle statistic based speckle reducing anisotropic diffusion method (PRSS-SRAD) [21] was proposed to solve the over-smoothing problem. The above anisotropic diffusion based filtering methods inefficiently use edge characteristics, resulting in either over-smoothing image or an image containing misinterpreted spurious edges. To alleviate such problems, a novel filter based on edge probability and pixel relativity-based speckle reducing anisotropic diffusion (EPPR-SRAD) [22] was proposed. The above filters use the diffusion coefficients where the low values are assigned to the edges & textures and high values are set to the homogeneous areas. As a consequence, the homogeneous areas are smoothed and the details such as the edges and textures, etc. are preserved. All of the above filters use all the samples in the local window for speckle filtering, they do not have the ability to perform selective filtering. Sigma filter [23] is a classical selective speckle filter, it trims the samples in the reference window with an upper and a lower threshold, and then mean filtering is applied to the trimmed samples. However, Sigma filter also blurs the edges, which influences the application of the SAR images. Based on the Sigma filtering methodology, Lee *et al.* [24] proposed an improved sigma filter, where Sigma filter was extended and improved by redefining the sigma range based on the speckle probability density functions. Improved sigma filter solves the deficiencies of the original sigma filter, and it is simple and efficient, however, it still destroys the details and blurs the images.

Non-local means based filters [25]–[29] are recently proposed and they achieve promising de-speckling performance. However, they greatly depend on the non-local intensity homogeneity. Block-matching and 3-D filter (BM3D) originally proposed by Dabov *et al.* [30] is aimed at the restoration of images corrupted by the additive white Gaussian noise (AWGN). It comprehensively uses the nonlocal patch-based estimation method with Wiener filtering and wavelet transforms, BM3D filter achieves an excellent AWGN filtering performance. However, BM3D filter cannot be directly applied to speckle noise reduction for SAR images. Parrilli *et al.* [31] adapted the model and architecture used in BM3D to the multiplicative noise of SAR speckle noise, the BM3D based de-speckling algorithm for SAR images (SAR-BM3D) was proposed. SAR-BM3D achieves a better de-speckling performance, however, its structure is complex and inefficient. Based on the theory of SAR-BM3D filter,

a non-local filter for SAR interferometric phase restoration called InSAR-BM3D [32] was proposed recently, it adapts the individual processing steps to the peculiarities of InSAR data. InSAR-BM3D greatly relies on proper phase-oriented solutions, the achieved filtering performance are based on the use of de-correlating transforms, development and testing methods based on the joint processing of all data should be further researched.

Bilateral filter developed by Tomasi and Manduchi [33] is a widely-used noise filtering method in optical images. Bilateral filter comprehensively exploits the similarity information of both gray levels and spatial location, it achieves a good smoothing performance for Gaussian noise while preserving the details such as edge and textures in optical images. However, bilateral filtering is not effective for impulse noise reduction, and speckle noise in SAR images are usually presented as impulse noise, especially for strong speckle. The reason why impulse noise cannot be effectively smoothed is because if the filtering samples contain impulse noise, and the intensity of the impulse noise is close to that of the pixel-under-filtering (PUF), so the impulse noise sample occupies the largest proportion in the filtered samples. As a consequence, the PUF of the strong speckle noise is enhanced instead of being smoothed.

Considering the limitations of the above de-speckling algorithms, this paper combines the advantages of bilateral filter and Sigma filter, a refined bilateral filtering algorithm based on adaptively-trimmed-statistics (ATS-RBF) of SAR images is proposed. Our main contributions are stated as follows:

1) Traditional bilateral filter uses all the samples in the local reference window to generate the combined similarity weights, the strong speckle noise presented as impulse noise cannot be reduced. The proposed ATS-RBF designs an adaptive threshold based method to trim the samples in the local reference window automatically, then the trimmed samples are used for bilateral filtering, so the strong speckle noise can be greatly smoothed.
2) As for Sigma filter [23], all the samples are trimmed with a fixed range of two-sigma. However, the speckle filtering of the detailed regions should focus on the edge preservation, a larger range should be designed to eliminate less samples. On the contrary, the filtering of the homogeneous regions should be emphasized on the speckle noise smoothing, so a smaller range is selected to eliminate much more samples. The proposed ATS-RBF designs an adaptive range for sample trimming, where the range depends on the homogeneity of the backgrounds. If the PUF is an edge pixel, a larger range is designed to sustain the image details. On the contrary, if the PUF is a speckle pixel, then a relatively lower range is assigned to smooth the speckle noise.
3) The proposed ATS-RBF designs an alterable window size for speckle noise filtering. The size of the window is adaptive to the homogeneity of the backgrounds, if the PUF is speckle in homogeneous area, the size of the window is assigned to a large value to smooth the speckle noise. On the contrary, if the PUF is the edge point, the size of the window is set to a small value to greatly preserve the edges and textures.
4) The proposed ATS-RBF can smooth the speckle noise while sustaining the details of the SAR images.

This remainder of this paper is arranged as follows: Section II proceeds to describe the proposed ATS-RBF based de-speckling methodology in detail, where traditional bilateral filtering methodology is briefed, moreover, the adaptive threshold based sample trimming, the trimming depth optimization, and the alterable window size based bilateral filtering are detailed. In Section III, experimental results are given with detailed analysis subjectively and objectively. Finally, Section IV concludes the paper.

II. THE PROPOSED ATS-RBF METHODOLOGY

Fig. 1 gives the flow chart of the proposed ATS-RBF. Inspired by the Sigma filtering method, we design an adaptive threshold based sample trimming method to trim the samples in the local reference window, then alterable window size based bilateral filtering is implemented to the PUF using the adaptively-trimmed samples.

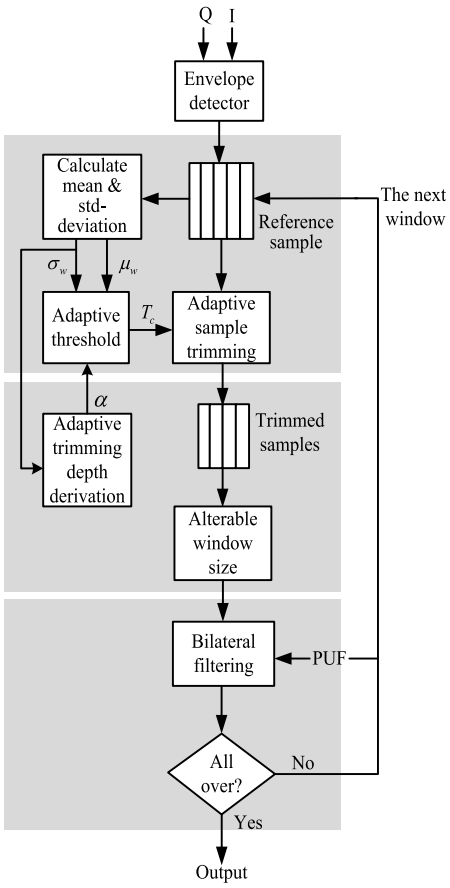

FIGURE 1. Flow chart of the proposed ATS-RBF for speckle reduction in SAR images.

A. TRADITIONAL BILATERAL FILTERING

As for the bilateral filter, the filtering weights are determined by the geometric closeness and photometric similarity, where these two are combined in the following formula [33]

$$h(x) = k^{-1}(x) \int_{-\infty}^{\infty} \int_{-\infty}^{\infty} f(\xi) \cdot c(\xi, x) \cdot s(f(\xi), f(x)) d\xi, \quad (1)$$

where $c(\xi, x)$ measures the geometric closeness between the PUF of x and its surrounding pixels ξ, $s(f(\xi), f(x))$ is the photometric similarity between the PUF of x and the surrounding pixels, $k^{-1}(x)$ is the normalization coefficient, and it is expressed as

$$k(x) = \int_{-\infty}^{\infty} \int_{-\infty}^{\infty} c(\xi, x) s(f(\xi), f(x)) d\xi. \quad (2)$$

Bilateral filter needs to design two weight functions including the geometric closeness similarity function and the photometric similarity function. The designation of these two weight functions directly affects the de-noising effect. The Gaussian kernel function is much more commonly used for both the geometric closeness function and the photometric similarity function. The Gaussian kernel function of geometric closeness weight is expressed as

$$c(\xi, x) = e^{-\frac{1}{2}\left(\frac{d(\xi, x)}{\sigma_d}\right)^2}, \quad (3)$$

where $d(\xi, x)$ is the Euclidean distance between the central pixel of x and its surrounding pixels ξ.σ_d is the geometric diffusion factor which controls the strength of low-pass filtering. The larger σ_d is, the stronger the low-pass filtering strength is, and the more blurred the filtering result will be. The window photometric similarity function is usually designed as

$$s(f(\xi), f(x)) = e^{-\frac{1}{2}\left(\frac{f(\xi) - f(x)}{\sigma_r}\right)^2}, \quad (4)$$

where σ_r is the photometric similarity diffusion factor. In order to get a good filtering result, σ_d and σ_r should be selected appropriately in order to achieve promising filtering results. Bilateral filter smooths the Gaussian noise while maintaining the image details. However, it cannot be applied directly to non-Gaussian noise, especially for the impulse noise. Fig. 2 is the filtering weights for the impulse noise. It can be seen that bilateral filter cannot smooth the strong impulse noise, but enhances it to some extent. This is because that if the filtering samples contain impulse noise, and the intensity of the impulse noise is close to that of the PUF, and they are spatially close, so the impulse noise sample occupies the largest proportion in the filtered samples. As a consequence, the strong speckle PUF cannot be smoothed, but enhanced.

B. ADAPTIVE-THRESHOLD BASED SAMPLE TRIMMING

Although bilateral filter preserves edges while smoothing the Gaussian noise, it cannot reduce the impulse noise. However, the speckle noise in SAR images is usually presented as impulse noise, especially for strong speckle. Therefore, we come over a mind of adjusting the photometric similarity

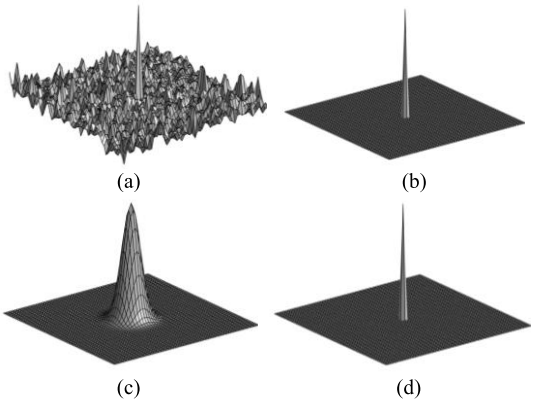

FIGURE 2. Filtering weights for the impulse noise. (a) is the local reference window with impulse noise in the center, (b) is the photometric similarity weights, (c) is the geometric closeness weights, (d) is the combined similarity weights.

weights based on the adaptively-trimmed-statistics to weaken the influence of the impulse noise sample.

Inspired by the Sigma filtering method [23], we intend to develop an adaptive-threshold based method for sample trimming, and the samples inside the restricted range are automatically kept through

$$I_{i,j} \in \psi, s\,t \cdot \left|I_{i,j} - \mu_w\right| \leq \alpha \cdot \sigma_w, \quad (5)$$

where $I_{i,j}$ is the intensity of the sample (i, j) in the reference window, α is the trimming depth, μ_w and σ_w are the mean and standard deviation of all the samples in the reference window, which are derived as

$$\mu_w = \frac{1}{N^2} \sum_{m=1}^{N} \sum_{n=1}^{N} I_{i,j}, \quad (6)$$

$$\sigma_w = \sqrt{\frac{1}{N^2} \sum_{m=1}^{N} \sum_{n=1}^{N} \left(I_{i,j} - \mu_w\right)^2}, \quad (7)$$

where N is the size of the local reference window.

If (5) is satisfied, the sample in the local reference window will be kept for bilateral filtering, otherwise, it is eliminated. After the adaptive-threshold based sample trimming, the combined filtering weights of $h(x)$ are generated through (1)-(4), where the original samples of ξ are replaced with the trimmed samples of ψ. Fig. 3 is an adaptive-threshold based sample trimming example, where the mean and the standard deviation are set to 68 and 15. The hatched area of Fig. 3 are the trimmed samples with a fixed trimming depth of $\alpha = 1.0$, and the samples outside the range are eliminated.

After the adaptive threshold based sample trimming of the local reference window, the adjusted photometric similarity weights of $s(f(\psi), f(x))$ and the combined similarity weights of $h(x)$ are shown in Fig. 4 (e) and (f). From which we can see that the combined similarity weights can greatly weaken the influence of the strong speckle noise, and the strong speckle presented as the impulse noise can be smoothed.

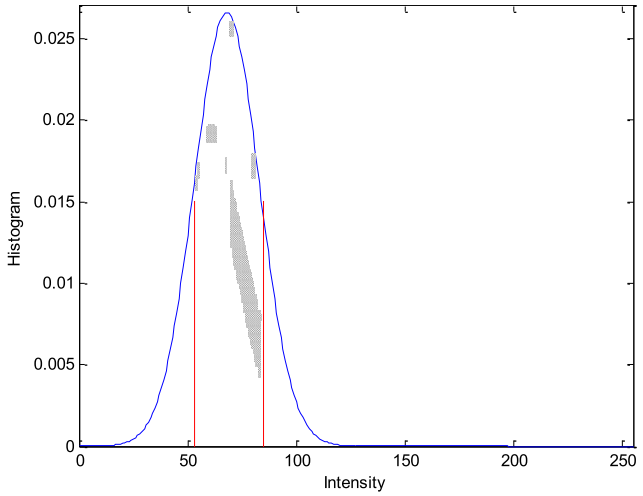

FIGURE 3. The hatched area are the trimmed samples with a fixed trimming depth of $\alpha = 1.0$.

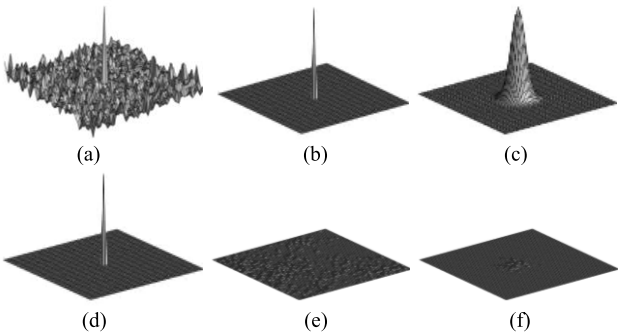

FIGURE 4. Filtering weights for the impulse noise. (a) is the original SAR image with impulse noise in the center, (b) is the photometric similarity weights of traditional bilateral filter, (c) is the geometric closeness weights, (d) is the combined similarity weights of traditional bilateral filter, (e) is the adjusted photometric similarity weights after sample trimming, and (f) is the adjusted combined similarity weights after sample trimming.

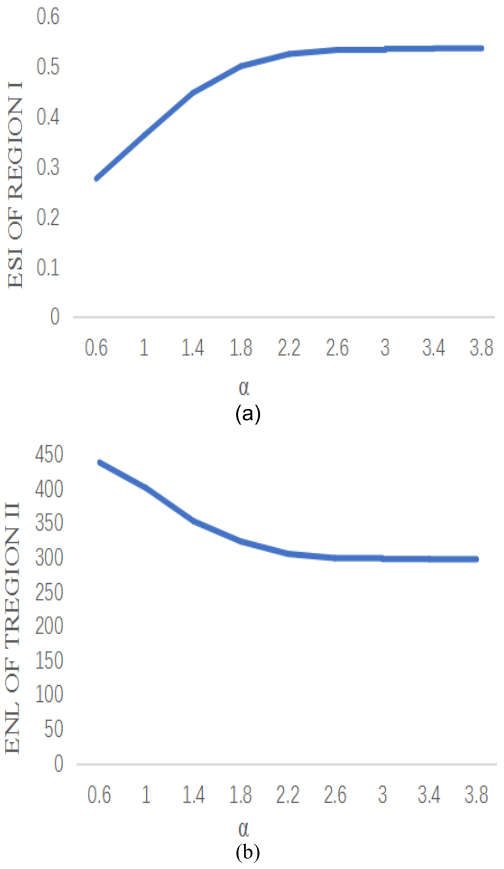

FIGURE 5. The filtering performance with different trimming depth of α. (a) The acquired values of ENL on a homogeneous region. (b) The acquired values of ESI on a detailed image.

The trimming depth is of great significance for the de-speckling performance, Fig. 5 illustrates the filtering performance of the trimmed statistics based bilateral filter under different trimming depths of α, where the speckle noise smoothing ability on a homogeneous region is evaluated using the Equivalent Number of Looks (ENL) [34], and the edge preservation capability on a detailed image is evaluated through the Edge Sustaining Index (ESI) [34]. It can be seen that if α is selected higher, then more samples are kept, the details will be greatly preserved, but the speckle reduction performance degrades.

In order to get both a promising speckle noise smoothing result and a good edge sustaining performance, here we design an automatic trimming depth kernel function through

$$\alpha = exp\left[\beta \cdot (\sigma_w/\sigma_h)^2\right], \tag{8}$$

where σ_w, σ_h are the standard deviations of the local reference window and the whole image, and β is the trimming strength weight. β controls the trimming strength, if it is selected lower, then the trimming is stronger. The adaptive values of α derived through (8) in Fig. 6 (a) used for experiments are shown in Fig. 6 (b). From Fig. 6 (b), it can be easily found that if the PUF is an edge pixel, σ_w is bigger than σ_h, then the trimming depth is assigned with a higher value, and fewer samples are eliminated, so the edges and textures can be well sustained. These pixels are labeled as the bright pixels of Fig. 6 (b). On the contrary, if the filtered pixel is a clutter pixel of the smooth region, then σ_w is smaller than σ_h, and the trimming depth is assigned with a relatively lower value, so more samples are removed, the speckle noise can be greatly smoothed. These are illustrated as the dark pixels in Fig.6 (b).

As can be seen from Fig.6, the trimming depth of α is larger in the edge & texture areas and smaller in the homogeneous areas. Combined with Fig. 5, a larger value of α means that more samples in the local reference window are kept and the edge details can be better preserved. But in the homogeneous regions, α is smaller, and more pixels that deviate from the mean value will be eliminated, such as the impulse noise. They do not participate in the construction of the photometric similarity weight. As a consequence, the adjusted combined similarity weights are much more precise, and the strong speckle noise can be smoothed while the details of the images are well sustained.

C. ALTERABLE WINDOW BASED REFINED BILATERAL FILTERING

In part B, the proposed ATS-RBF designs an adaptive-threshold-based sample trimming scheme to adaptively smooth the speckle noise while sustaining the image details. In bilateral filtering, in order to enhance the effect of smoothing noise, larger values of the diffusion factors of σ_d and σ_r should be specified. However, this will result in the loss of the image details. To further smooth the speckle noise in the homogeneous regions while preserving the image details, we propose an alterable window size based filtering method. Firstly, a window size of r_w is initiated, the standard deviation of the local reference window σ_w, and the standard deviation of the whole image σ_h are derived. The window size is enlarged when the following condition is satisfied

$$(\sigma_w/\sigma_h)^2 \leq T, \tag{9}$$

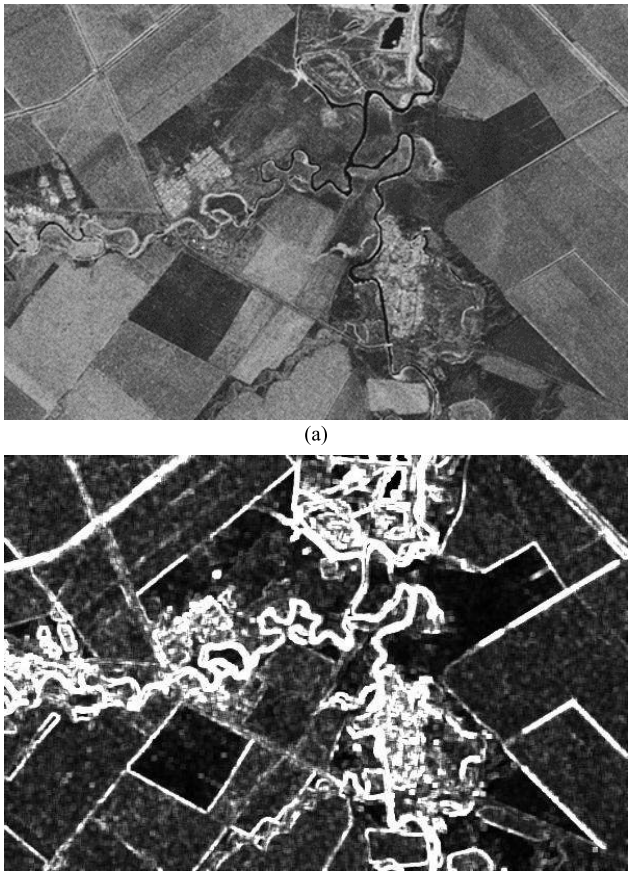

(a)

(b)

FIGURE 6. The adaptive values of the trimming depths derived through (8), (a) the original TerraSAR-X image, (b) the adaptive values of the trimming depth, where the edge points are automatically assigned with higher values, which are presented as the bright pixels.

where T is the expansion threshold, which controls the window size. According to the Fig. 6, we know that the ratio of σ_w to σ_h indicates the homogeneity of the region. The value of σ_w/σ_h is larger in the detailed region and smaller in the homogeneous region. If (9) is satisfied, then the local reference window is homogeneous, and the window size of the local reference window can be enlarged through

$$r_w = r_w + 2^i \tag{10}$$

where i is the round number. The size of the window increases if (9) is satisfied, and it grows with a step of 2. However, the growth ceases when (9) is not met. This can be explained by the reason that when the extended local reference window is still homogeneous without edges, then the size can be enlarged to smooth the speckle noise much stronger. However, when the extended window contains details such as edges & textures, then (9) is no longer satisfied, and the size will not be extended to sustain the image details.

The main steps of the proposed ATS-RBF are detailed as follows:

Step 1) The initial size of the local reference window of r_w, the expansion threshold of T, the diffusion factors of σ_d and σ_r, and the trimming strength weight of β are initiated.

Step 2) The standard deviations of the local reference window and the whole image are derived, and the window size of the local reference window increases if (9)-(10) are met. The final window size is acquired if (9) is not satisfied.

Step 3) The sample trimming depth of α is derived through (8), and the samples in the local reference window are adaptively trimmed through (5)-(7).

Step 4) The photometric similarity kernel weights of $s(x)$ are calculated using the adaptively-trimmed samples as shown in (4).

Step 5) Then, the combined bilateral filtering weights of $h_(x)$ are calculated through (1)-(3), and bilateral filtering is implemented to the PUF.

Step 6) If it is the end of the whole input image, output the filtering result. Otherwise, move on to the next pixel and repeat the processes from Step 2) to Step 5).

III. EXPERIMENTS AND ANALYSIS

A. PERFORMANCE EVALUATION METRICS

1) EQUIVALENT NUMBER OF LOOKS (ENL) [34]

ENL is an index to measure the relative intensity of speckle noise smoothing in SAR images, which is defined as

$$ENL = \frac{E^2(I)}{\sigma^2(I)}, \tag{11}$$

where $E(I)$ and $\sigma(I)$ are the mean and standard deviation of the filtered SAR image.

2) PEAK SIGNAL-TO-NOISE RATIO (PSNR) [35]

PSNR (in decibel) is the ratio between the maximum power of the signal and that of the noise. PSNR is derived as

$$PSNR = 10 \cdot log_{10}\left(\frac{x^2_{max}}{MSE}\right), \tag{12}$$

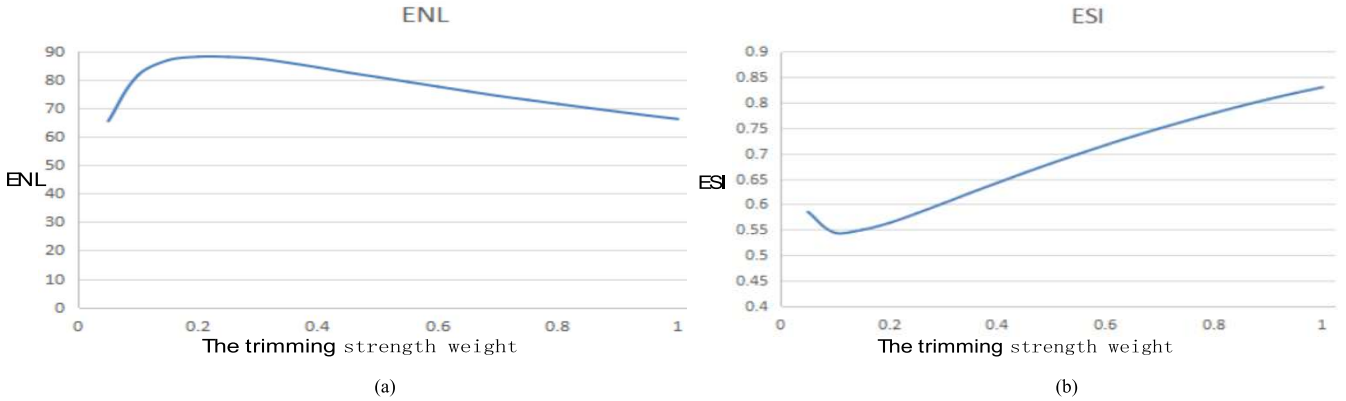

FIGURE 7. The de-speckle performance on speckle-contaminated simulated Boat image of the proposed ATS-RBF using different values of β with a fixed window size of 5×5. (a) is the acquired values of ENL, (b) is the acquired values of ESI. In the image.

where x_{max} is the maximum value of the data format, and MSE is the mean-square error, which is expressed as

$$MSE = \frac{1}{m \cdot n} \sum_{i=1}^{m} \sum_{j=1}^{n} \left| I'_{i,j} - I_{i,j} \right|^2. \tag{13}$$

3) STRUCTURAL SIMILARITY METRIC (SSIM) [36]

SSIM is a metric to evaluate the speckle filtering quality that measures the similarity between the original SAR images and the filtered image, it is defined as

$$SSIM = \frac{\left(2\mu_x\mu_y + c_1\right) \cdot \left(2\sigma_x\sigma_y + c_2\right)}{\left(\mu_x^2 + \mu_y^2 + c_2\right) \cdot \left(\sigma_x^2 + \sigma_y^2 + c_2\right)}, \tag{14}$$

where μ_x and μ_y are the mean values of the original image and the filtered result, σ_x and σ_y are the standard deviation values of the original image and the filtered result, c_1 and c_2 are used to stabilize the division that can occur with a weak denominator.

A high ENL indicates a strong speckle noise smoothing capability, a larger value of PSNR represents a smaller loss, SSIM values at the range of [0, 1], and the SSIM closer to 1 indicates a higher similarity.

B. SPECKLE FILTERING EXPERIMENTS AND ANALYSIS

Traditional speckle noise filters such as the Lee filter [13], the SRAD filter [18], the Sigma filter [23], the improved Sigma filter [24], and the SAR-BM3D filter [31] are selected for speckle reduction performance comparison and evaluation. Furthermore, traditional bilateral filter [33] is used for comparison to validate the better filtering performance of the proposed ATS-RBF. The simulation parameters are set as follows:

1) Comprehensively considering the speckle smoothing and the image detail sustaining, the window sizes of all the filters except for the proposed ATS-RBF are set to 5×5. The filters can better sustain the image details while smoothing the speckle noise. ATS-RBF designs an alterable-window-size based filtering method to smooth the speckle noise while sustaining the details.
2) As for SRAD [18], the time step size of Δt is set to 0.08, the scaling factor of k is set to 3.
3) Sigma filter [23] is based on the two-sigma probability of Gaussian distribution, 95.5% pixels in the local reference window are kept for filtering.
4) As for the improved Sigma filter, the parameters are set the same to [24] for the multi-look SAR images, the percentile value of Z is set to 98%, the sigma value of ξ is specified to 0.9, and the threshold of the strong reflective pixel in the window T_k is set to 6.0.
5) The same to the parameter setting of SAR-BM3D in [31], the similarity weight value of γ is equal to 1.
6) Both of the geometric diffusion factor of σ_d and the photometric similarity diffusion factor of σ_r of the traditional bilateral filter [33] and the proposed ATS-RBF are set to 3.0 and 40, respectively.
7) As for the proposed ATS-RBF, the initial window size is set to 5×5. The trimming strength weight of β is of great importance to the filtering performance, if it is selected too high, then the trimming is weaker, and more samples are used for bilateral filtering, the speckle noise cannot be smoothed. Accordingly, if it is selected too low, then the trimming is stronger, and less samples participate in bilateral filtering, the image details will be ruined. We conducted experiments on the speckle-contaminated Boat image using different values of β with a fixed window size of 5×5, and the acquired values of ENL, and ESI are recorded, as shown in Fig. 7. Comprehensively considering the speckle smoothing and the image detail sustaining, we use an optimal value of 0.5 for test in this part.
8) As for the proposed ATS-RBF, The window expansion threshold of T is of great importance to the speckle smoothing performance. We conducted experiments on the speckle-contaminated Boat image using different values of T with a fixed trimming strength weight of $\beta = 0.5$, and the acquired values of ENL, and ESI are recorded, as shown in Fig. 8. Comprehensively considering the speckle smoothing and the image detail

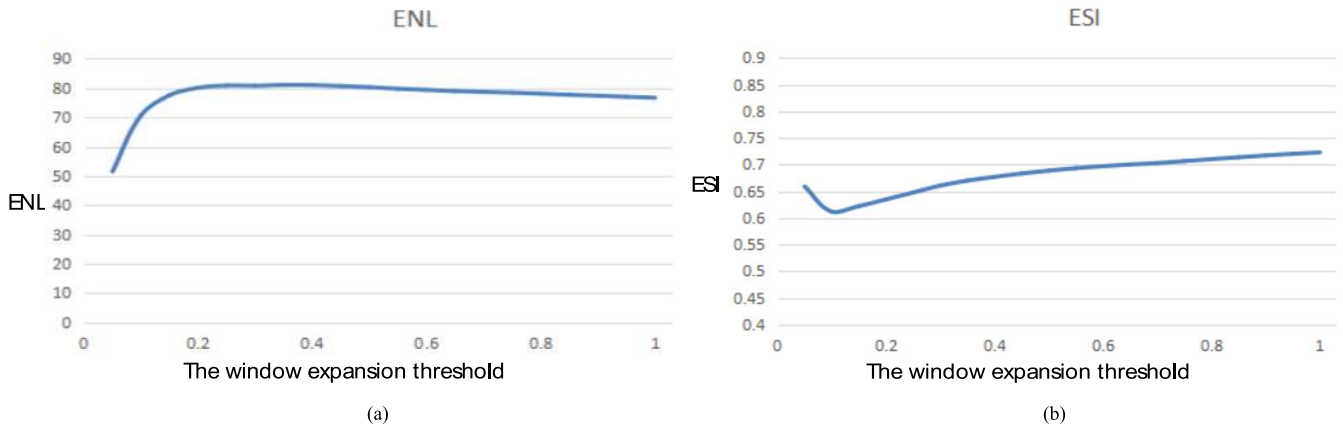

FIGURE 8. The de-speckle performance on speckle-contaminated simulated Boat image of the proposed ATS-RBF using different values of T with a fixed trimming strength weight of. (a) is the acquired values of ENL, (b) is the acquired values of ESI.

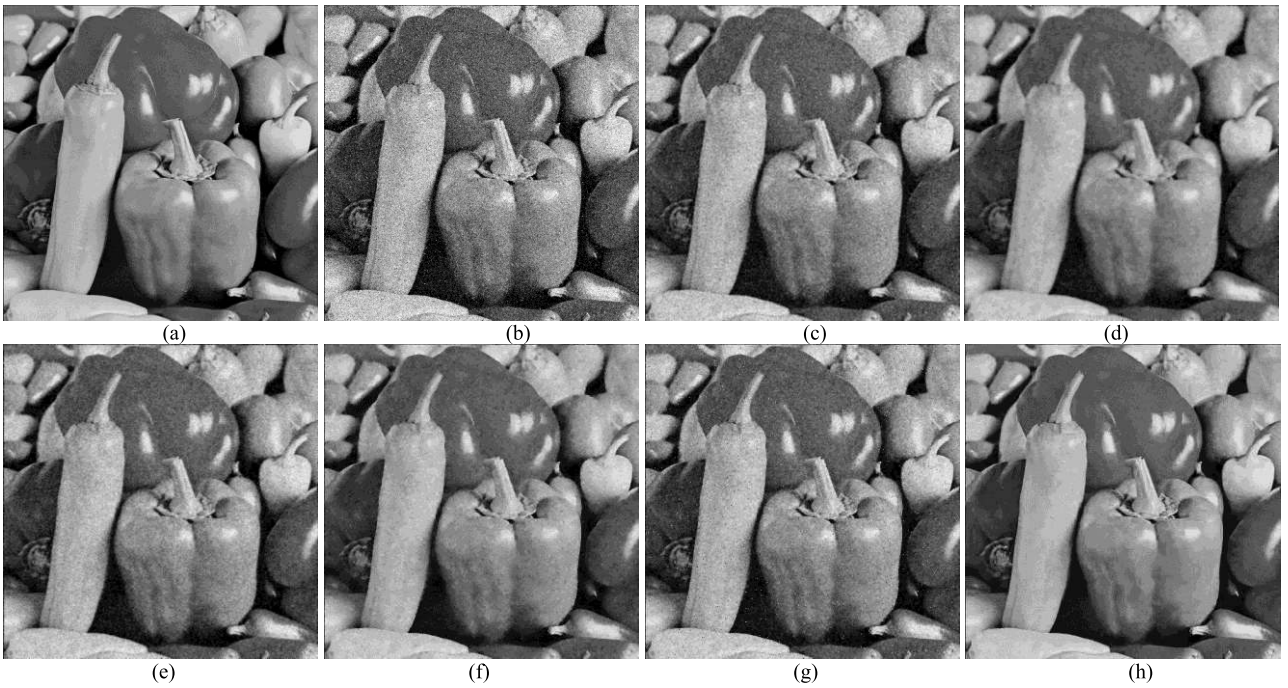

FIGURE 9. The speckle reduction performance on speckle-noise-contaminated simulated Peppers image with detailed edges. (a) is the noise-free simulated SAR image, (b) is the speckle-noise-contaminated image, (c) is the result of Lee filter [13], (d) is the result of SRAD filter [18], (e) is the result of Sigma filter [23], (f) is the result of SAR-BM3D filter [31], (g) is the result of traditional bilateral filter [33], and (h) is the result of the proposed ATS-RBF filter.

sustaining, we use an optimal value of 0.25 for test in this part.

The experiments are implemented on the simulated images and real TerraSAR-X data, and the de-speckling performance of the traditional filters and the proposed ATS-RBF are compared and analyzed in detail. Moreover, the de-speckling performance of ATS-RBF is evaluated subjectively and objectively. The experiments on the simulated data and real SAR data are presented in Part B.1 and Part B.2.

C. EXPERIMENTS ON SIMULATED SAR DATA

In order to evaluate the de-speckling performance of the proposed ATS-RBF, the standard reference image of Peppers illustrated in Fig. 9 (a) is used for experiments. The original Peppers image is added with multiplicative speckle noise following Rayleigh distribution.

As shown in Fig. 9, (a) is the noise-free image, where detailed information are presented. Fig. 9 (b) is the speckle noise contaminated image. Fig. 9 (c) to Fig. 9 (h) shows the speckle filtering results by different filters. The corresponding values of ENL, PSNR and SSIM are recorded, as shown in TABLE 1.

As can be seen from Fig. 9, traditional de-speckling filters such as Lee, SRAD, Sigma, and Improved Sigma can smooth the speckle noise in a certain level, but they ruin the image details with low values of SSIM and PSNR.

TABLE 1. The objective de-speckling performance evaluation of different filters on the speckle-noise contaminated Peppers image.

Filters \ Metrics	ENL	PSNR	SSIM
Lee [13]	5.28	26.39	0.33
SRAD [18]	5.06	23.07	0.27
Sigma [23]	5.11	26.76	0.34
Improved Sigma [24]	4.92	24.03	0.30
SAR-BM3D [31]	5.23	28.52	0.40
Bilateral filter [33]	4.87	23.58	0.29
The proposed ATS-BF	**5.31**	**29.25**	**0.43**

Traditional bilateral filter cannot smooth the strong speckle noise which are often presented as impulse noise, it acquires the lowest value of ENL. SAR-BM3D can smooth the speckle noise while sustaining the image details as illustrated in Fig. 9 (h). However, SAR-BM3D has a poorer performance compared with the proposed ATS-RBF filter. The proposed ATS-RBF filter comprehensively uses the spatial closeness similarity and the photometric similarity, an adaptive-threshold based sample trimming method is designed to smooth the speckle noise and sustain the image details, it acquires the highest values of PSNR and SSIM compared with other filters. Furthermore, an alterable-window-size scheme is proposed to enhance the smoothing strength in the homogeneous regions, it achieves the highest value of ENL compared to other filters. From Fig. 9 and TABLE 1, the proposed ATS-RBF has a better de-speckling performance both on speckle noise smoothing and image detail preservation.

D. EXPERIMENTS ON THE TERRASAR-X DATA

TerraSAR-X SAR images shown in Fig. 10 are used for experiments. Fig. 10 is the firstly acquired image of TerraSAR-X over the Volga delta of south Russia on June 19, 2007 through the Strip-Map (SM) imaging mode, of which the resolution is 3 meter, the polarization is HH, and effective number of looks is 8.3. Two regions marked by the white boxes of Fig. 10 are selected, furthermore, the right white box marked region in Fig. 10 is enlarged separately as illustrated in Fig. 11. Two types of sub-regions marked by the white boxes of Fig. 11 are selected, one is the detailed region labeled as REGION III with rich edges to validate the edge preservation capability of the proposed ATS-RBF. The other are the homogeneous regions labeled as REGION I, REGION II of Fig. 11 and Fig. 13 (a) to evaluate the speckle noise smoothing performance of the proposed ATS-RBF.

FIGURE 10. TerraSAR-X image used for experiments, of which is acquired by the SM mode of X-band TerraSAR-X over the Volga region of south Russia on June 19, 2007. The resolution is 3 meter, and the polarization is HH, the effective number of looks is 8.3.

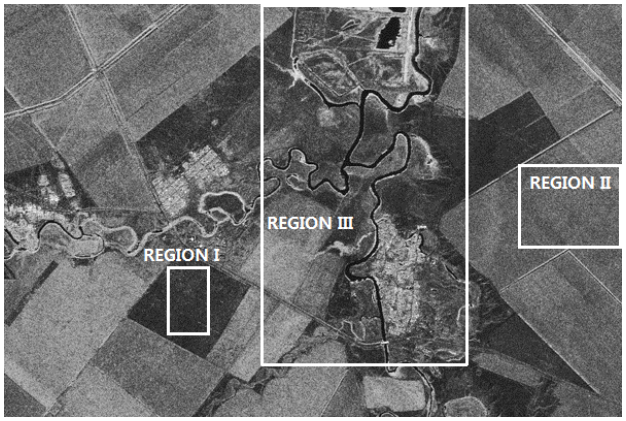

FIGURE 11. Detailed SAR image used for de-speckling performance validation.

In order to show the edge preservation performance of each filtering algorithm, the filtering results of REGION III of Fig. 11 are illustrated in Fig. 12. The corresponding values of ENL of different filters on the homogeneous regions of REGION I, REGION II of Fig. 11, and Fig. 13 (a) are listed in TABLE 2.

TABLE 2. The speckle smoothing performance of the homogeneous regions evaluated by the ENL.

Filters \ Images	REGION I of Fig. 11	REGION II of Fig. 11	Fig. 13 (a)
Lee [13]	60.5	114.6	18.1
SRAD [18]	60.1	126.0	18.0
Sigma [23]	55.9	111.5	18.1
Improved Sigma [24]	58.7	110.9	17.8
SAR-BM3D [31]	112.4	188.8	18.1
Bilateral filter [33]	71.8	135.0	17.8
The proposed ATS-BF	**112.9**	**190.2**	**18.3**

De-speckling filters such as Lee, Sigma, Improved Sigma, and SRAD reduce the speckle noise in a certain level, however, they blur the image details as shown in Fig. 12 (b) to Fig. 12 (e), and Fig. 13 (b) to Fig. 13 (e). They all

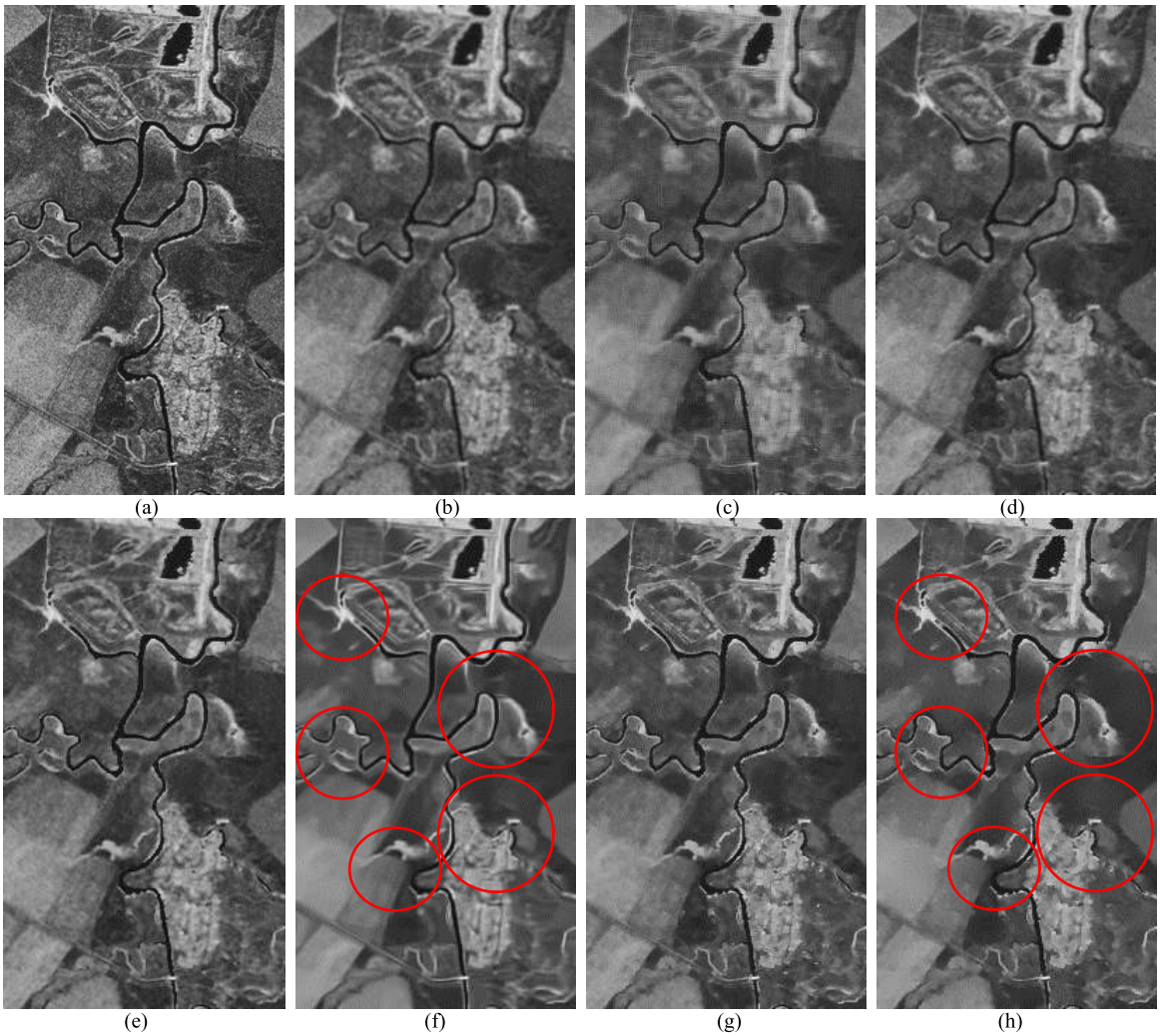

FIGURE 12. The speckle reduction performance on TerraSAR-X image with detailed edges and textures. (a) is the original TerraSAR-X image, (b) is the result of Lee filter [13], (c) is the result of SRAD filter [18], (d) is the result of Sigma filter [23], (e) is the result of improved Sigma filter [24], (f) is the result of SAR-BM3D filter [31], (g) is the result of traditional bilateral filter [33], and (h) is the result of the proposed ATS-RBF filter.

acquire much lower values of ENL as shown in TABLE 2. Traditional bilateral filter has a good edge sustaining ability, however, it cannot smooth the strong speckle noise as shown in Fig. 12 (g). Both SAR-BM3D and the proposed ATS-RBF have excellent speckle noise smoothing and edge preservation performance, they acquire much higher values of ENL compared with other filters, as listed in TABLE 2. However, ATS-RBF has a better speckle noise smoothing performance compared to SAR-BM3D. Moreover, ATS-RBF has a better edge sustaining performance on detailed SAR images, which is illustrated in the red-circle marked areas of Fig. 12 (f) and Fig. 12 (h). The image details can be better sustained by ATS-RBF compared to SAR-BM3D.

According to Fig. 9, Fig. 12, Fig. 13, TABLE 1, and TABLE 2, we can draw the conclusion:

1) Traditional filters such as Lee, SRAD, Sigma, Improved Sigma can smooth the speckle noise in a certain level, but they ruin the details of the images, they acquire very low values of SSIM.

2) Traditional bilateral filter uses all the samples in the local reference window for photometric similarity weights generation. However, it cannot smooth the strong speckle noise in SAR images, but enhances it instead.

3) The proposed ATS-RBF designs an adaptive-threshold based sample trimming method to eliminate the strong speckle noise sample which influences the accuracy of the photometric similarity weights. Furthermore, an alterable window size based method is proposed to enhance the smoothing strength in homogeneous regions. ATS-RBF has a better speckle noise smoothing capability, and a better edge sustaining performance compared to SAR-BM3D

4) In summary, the refined bilateral filtering method based on the adaptively-trimmed-statistics proposed by this paper can effectively smooth the speckle noise and

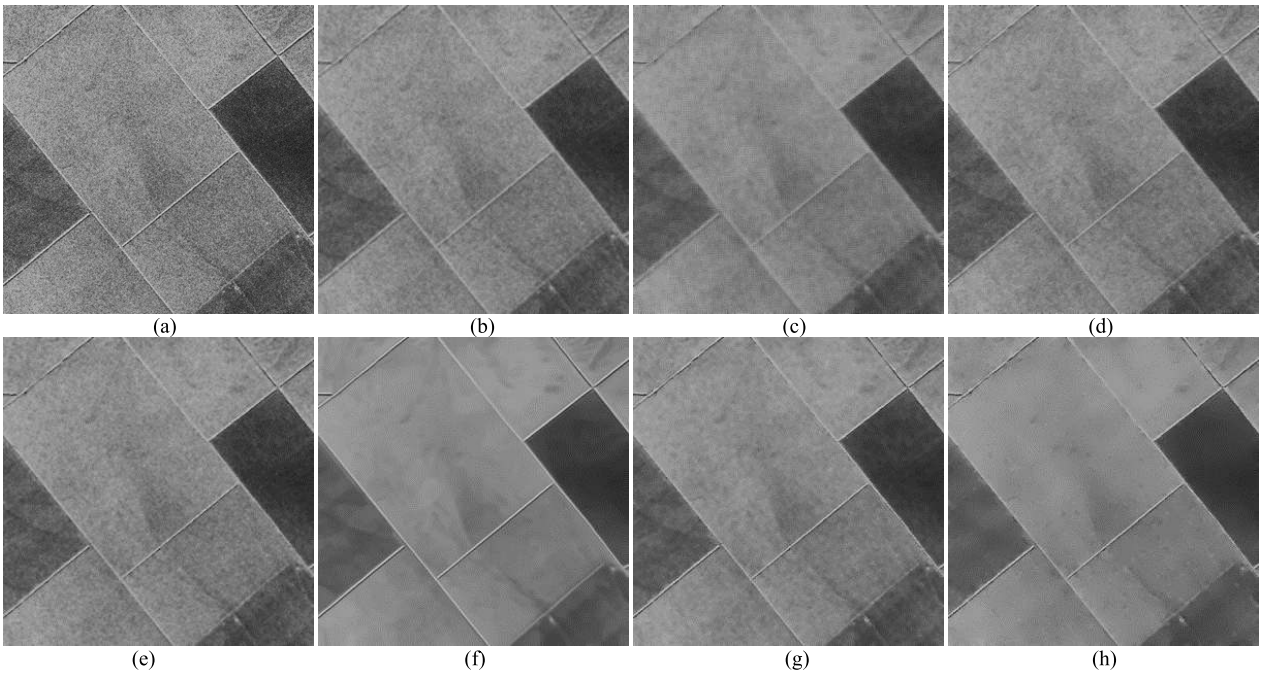

FIGURE 13. The speckle noise smoothing performance on the homogeneous region. (a) is the original TerraSAR-X image, (b) is the result of Lee filter [13], (c) is the result of SRAD filter [18], (d) is the result of Sigma filter [23], (e) is the result of improved Sigma filter [24], (f) is the result of SAR-BM3D filter [31], (g) is the result of traditional bilateral filter [33], and (h) is the result of the proposed ATS-RBF filter.

maintain the edge & texture information of the SAR images.

IV. CONCLUSION

Combining the advantages of bilateral filter and Sigma filter, this paper proposes a refined bilateral filtering method based on the adaptive-trimmed-statistics. ATS-RBF designs an adaptive threshold based method to adaptively trim the samples in the local reference window, so the photometric similarity weights are adjusted by eliminating the data samples outside of the range to weaken the influence of the strong impulse noise. The trimming depth is automatically generated according to the homogeneity of the filtered pixel. Furthermore, an alterable window size based method is proposed to enhance the speckle noise smoothing strength in homogeneous regions. ATS-RBF has an excellent speckle noise smoothing and edge sustaining performance. ATS-RBF has a great application value in SAR image interpretation.

ACKNOWLEDGEMENTS

The authors would like to thank the editor, the associate editor, and the anonymous reviewers for their constructive work that significantly elevate the content of this paper.

REFERENCES

[1] J. Jiao, Y. Zhang, H. Sun, X. Yang, X. Gao, W. Hong, K. Fu, and X. Sun, "A densely connected end-to-end neural network for multiscale and multiscene SAR ship detection," *IEEE Access*, vol. 6, pp. 20881–20892, Apr. 2018.

[2] J. Deng, Y. Ban, J. Liu, L. Li, X. Niu, and B. Zou, "Hierarchical segmentation of multitemporal RADARSAT-2 SAR data using stationary wavelet transform and algebraic multigrid method," *IEEE Trans. Geosci. Remote Sens.*, vol. 52, no. 7, pp. 4353–4363, Jul. 2014.

[3] H. S. Jung, Z. Lu, and L. Zhang, "Feasibility of along-track displacement measurement from sentinel-1 interferometric wide-swath mode," *IEEE Trans. Geosci. Remote Sens.*, vol. 51, no. 1, pp. 573–578, Jan. 2013.

[4] J. Chen, H. Lin, and Z. Pei, "Application of ENVISAT ASAR data in mapping rice crop growth in Southern China," *IEEE Geosci. Remote Sens. Lett.*, vol. 4, no. 3, pp. 431–435, Jul. 2007.

[5] L. Pulvirenti, N. Pierdicca, G. Boni, M. Fiorini, and R. Rudari, "Flood damage assessment through multitemporal COSMO-Skymed data and hydrodynamic models: The Albania 2010 case study," *IEEE J. Sel. Topics Appl. Earth Observ. Remote Sens.*, vol. 7, no. 7, pp. 2848–2855, Jul. 2014.

[6] W. Ao, F. Xu, Y. Li, and H. Wang, "Detection and discrimination of ship targets in complex background from spaceborne ALOS-2 SAR images," *IEEE J. Sel. Topics Appl. Earth Observ. Remote Sens.*, vol. 11, no. 2, pp. 536–550, Feb. 2018.

[7] Y. Sharay and U. Naftaly, "TECSAR: Design considerations and programme status," *IEE Proc.-Radar, Sonar Navigat.*, vol. 153, no. 2, pp. 117–121, Apr. 2006.

[8] J. Wang, H. Wang, W. Shao, J. Zhu, and X. Yuan, "Significant wave height retrieval from Gaofen-3 wave mode images," in *Proc. IEEE Int. Geosci. Remote Sens. Symp. (IGARSS)*, Valencia, Spain, Jul. 2018, pp. 3204–3207.

[9] J. S. Lee, L. Jurkevich, P. Dewaele, P. Wambacq, and A. Oosterlinck, "Speckle filtering of synthetic aperture radar images: A review," *Remote Sens. Rev.*, vol. 8, no. 4, pp. 313–340, 1994.

[10] R. M. Goldstein, H. A. Zebker, and C. L. Werner, "Satellite radar interferometry: Two-dimensional phase unwrapping," *Radio Sci.*, vol. 23, no. 4, pp. 713–720, Aug. 1988.

[11] G. Liu, S. Huang, A. Torre, and F. Rubertone, "Optimal speckle reduction in multi-look polarimetric SAR image," in *Proc. IEEE Int. Geosci. Remote Sens. Symp. (IGARSS)*, Florence, Italy, Jul. 1995, pp. 664–666.

[12] G. Liu, S. Huang, A. Torre, and F. Rubertone, "Optimal multi-look polarimetric speckle reduction and its effect on terrain classification," in *Proc. IEEE Int. Geosci. Remote Sens. Symp. (IGARSS)*, Lincoln, NE, USA, May 1996, pp. 1571–1573.

[13] J.-S. Lee, "Digital image enhancement and noise filtering by use of local statistics," *IEEE Trans. Pattern Anal. Mach. Intell.*, vol. PAMI-2, no. 2, pp. 165–168, Mar. 1980.

[14] J.-S. Lee, "Refined filtering of image noise using local statistics," *Comput. Graph. Image Process.*, vol. 15, no. 4, pp. 380–389, 1981.
[15] V. S. Frost, J. A. Stiles, K. S. Shanmugan, and J. C. Holtzman, "A model for radar images and its application to adaptive digital filtering of multiplicative noise," *IEEE Trans. Pattern Anal. Mach. Intell.*, vol. PAMI-4, no. 2, pp. 157–166, Mar. 1982.
[16] D. T. Kuan, A. A. Sawchuk, T. C. Strand, and P. Chavel, "Adaptive noise smoothing filter for images with signal-dependent noise," *IEEE Trans. Pattern Anal. Mach. Intell.*, vol. PAMI-7, no. 2, pp. 165–177, Mar. 1985.
[17] D. Kuan, A. Sawchuk, T. Strand, and P. Chavel, "Adaptive restoration of images with speckle," *IEEE Trans. Acoust., Speech, Signal Process.*, vol. 35, no. 3, pp. 373–383, Mar. 1987.
[18] Y. Yu and S. T. Acton, "Speckle reducing anisotropic diffusion," *IEEE Trans. Image Process.*, vol. 11, no. 11, pp. 1260–1270, Nov. 2002.
[19] S. Aja-Fernández and C. Alberola-López, "On the estimation of the coefficient of variation for anisotropic diffusion speckle filtering," *IEEE Trans. Image Process.*, vol. 15, no. 9, pp. 2694–2701, Sep. 2006.
[20] K. Krissian, C.-F. Westin, R. Kikinis, and K. G. Vosburgh, "Oriented speckle reducing anisotropic diffusion," *IEEE Trans. Image Process.*, vol. 16, no. 5, pp. 1412–1424, May 2007.
[21] G. Ramos-Llordén, G. Vegas-Sánchez-Ferrero, M. Martin-Fernández, C. Alberola-López, and S. Aja-Fernández, "Anisotropic diffusion filter with memory based on speckle statistics for ultrasound images," *IEEE Trans. Image Process.*, vol. 24, no. 1, pp. 345–358, Jan. 2015.
[22] D. Mishra, S. Chaudhury, M. Sarkar, A. S. Soin, and V. Sharma, "Edge probability and pixel relativity-based speckle reducing anisotropic diffusion," *IEEE Trans. Image Process.*, vol. 27, no. 2, pp. 649–664, Feb. 2018.
[23] J.-S. Lee, "A simple speckle smoothing algorithm for synthetic aperture radar images," *IEEE Trans. Syst., Man, Cybern.*, vol. SMC-13, no. 1, pp. 85–89, Jan./Feb. 1983.
[24] J.-S. Lee, J.-H. Wen, T. L. Ainsworth, K.-S. Chen, and A. J. Chen, "Improved sigma filter for speckle filtering of SAR imagery," *IEEE Trans. Geosci. Remote Sens.*, vol. 47, no. 1, pp. 202–213, Jan. 2009.
[25] W. G. Zhang and Q. Zhang, "SAR image despeckling combining target detection with improved nonlocal means," *Electron. Lett.*, vol. 47, no. 12, pp. 724–725, Jun. 2011.
[26] C. Jojy, M. S. Nair, G. R. K. S. Subrahmanyam, and R. Riji, "Discontinuity adaptive non-local means with importance sampling unscented Kalman filter for de-speckling SAR images," *IEEE J. Sel. Topics Appl. Earth Observ. Remote Sens.*, vol. 6, no. 4, pp. 1964–1970, Aug. 2013.
[27] R. Sharma and R. K. Panigrahi, "Improved patch-based NLM PolSAR speckle filter based on iteratively re-weighted least squares method," *IET Radar, Sonar Navigat.*, vol. 12, no. 1, pp. 30–36, Jan. 2018.
[28] G.-T. Li, C.-L. Wang, P.-P. Huang, and W.-D. Yu, "SAR image despeckling using a space-domain filter with alterable window," *IEEE Geosci. Remote Sens. Lett.*, vol. 10, no. 2, pp. 263–267, Mar. 2013.
[29] D. Tong, H. Yang, J. Wu, and J. Yang, "An improved non-local means filter for SAR image despeckle based on heterogeneity measurement," in *Proc. IEEE Int. Geosci. Remote Sens. Symp. (IGARSS)*, Valencia, Spain, Jul. 2018, pp. 2801–2804.
[30] K. Dabov, A. Foi, V. Katkovnik, and K. Egiazarian, "Image denoising by sparse 3-D transform-domain collaborative filtering," *IEEE Trans. Image Process.*, vol. 16, no. 8, pp. 2080–2095, Aug. 2007.
[31] S. Parrilli, M. Poderico, C. V. Angelino, and L. Verdoliva, "A nonlocal SAR image denoising algorithm based on LLMMSE wavelet shrinkage," *IEEE Trans. Geosci. Remote Sens.*, vol. 52, no. 2, pp. 606–616, Feb. 2012.
[32] F. Sica, D. Cozzolino, X. X. Zhu, L. Verdoliva, and G. Poggi, "InSAR-BM3D: A nonlocal filter for SAR interferometric phase restoration," *IEEE Trans. Geosci. Remote Sens.*, vol. 56, no. 6, pp. 3456–3467, Jun. 2018.
[33] C. Tomasi and R. Manduchi, "Bilateral filtering for gray and color images," in *Proc. 6th IEEE Int. Conf. Comput. Vis. (ICIP)*, Bombay, India, Jan. 1998, pp. 839–846.
[34] Y. Sheng and Z.-G. Xia, "A comprehensive evaluation of filters for radar speckle suppression," in *Proc. IEEE Int. Geosci. Remote Sens. Symp. (IGARSS)*, Lincoln, NE, USA, May 1996, pp. 1559–1561.
[35] Y.-H. Shiao, T.-J. Chen, K.-S. Chuang, C.-H. Lin, and C.-C. Chuang, "Quality of compressed medical images," *J. Digit. Imag.*, vol. 20, no. 2, pp. 149–159, Jun. 2007.
[36] Z. Wang, A. C. Bovik, H. R. Sheikh, and E. P. Simoncelli, "Image quality assessment: From error visibility to structural similarity," *IEEE Trans. Image Process.*, vol. 13, no. 4, pp. 600–612, Apr. 2004.

JIAQIU AI (M'17) was born in Ji'an, Jiangxi, in 1985. He received the B.S. degree in electronics and information from the Beijing Information Science and Technology University, in 2007, and the Ph.D. degree in information and communication from the University of Chinese Academy of Sciences, in 2012. He served as a Senior Engineer at the 38th Institute, China Electronic Technology Group Corporation (CETC), from 2012 to 2016. He is currently an Associate Professor with the Hefei University of Technology, Anhui, China. He has authored more than 20 journal papers. His current research interests include SAR image processing, radar target detection, and radar system design. He is invited as the Reviewer for the IEEE TRANSACTIONS ON GEOSCIENCE AND REMOTE SENSING, the IEEE JOURNAL OF SELECTED TOPICS IN APPLIED EARTH OBSERVATIONS AND REMOTE SENSING, the IEEE GEOSCIENCE AND REMOTE SENSING LETTERS, the *International Journal of Remote Sensing*, and *Signal Processing*.

RUIMING LIU was born in Fujian, in 1998. He is currently pursuing the B.Eng. degree with the Hefei University of Technology. His research interests include remote sensing image processing and artificial intelligence.

BO TANG received the Ph.D. degree in electrical engineering from the University of Rhode Island, Kingstown, RI, USA, in 2016. From 2016 to 2017, he was an Assistant Professor with the Department of Computer Science, Hofstra University, Hempstead, NY, USA. He is currently an Assistant Professor with the Department of Electrical and Computer Engineering, Mississippi State University. His research interests include the general areas of statistical machine learning and data mining, and their various applications in cyber-physical systems, including robotics, autonomous driving, and remote sensing.

LU JIA was born in 1988. She received the B.S. degree in electronic engineering from the China University of Petroleum, Qingdao, China, in 2011, and the Ph.D. degree in signal and information processing from Xidian University, Xi'an, China, in 2016. She is currently a Lecturer with the School of Computer and Information, Hefei University of Technology. Her main research interest includes remote sensing image change detection.

JINLING ZHAO received the B.Eng. and M.Eng. degrees from the Taiyuan University of Technology, China, in 2003 and 2006, respectively, and the Ph.D. degree from the University of Chinese Academy of Sciences, China, in 2010. From 2010 to 2013, he was a Postdoctoral Research Fellow jointly supported by the Institute of Remote Sensing and Digital Earth, Chinese Academy of Sciences, and the Beijing Academy of Agriculture and Forestry Sciences, China. He is currently an Associate Professor and the Office Administrator of the National Joint Engineering Research Center for Analysis and Application of Agro-Ecological Big Data, Anhui University. His research interests include remote sensing image processing, precision agriculture, and automated interpretation of land use and land cover (LULC).

FANG ZHOU (M'15) was born in Chizhou, Anhui, China, in 1986. She received the B.S. and Ph.D. degrees in information and communication from Xidian University, Xi'an, China, in 2009 and 2014, respectively. She is currently a lecturer with the School of Computer and Information, Hefei University of Technology, Hefei, Anhui. Her current research interests include synthetic aperture radar signal processing and SAR imaging signal correction.